

## rTg-D: A novel transgenic rat model of cerebral amyloid angiopathy Type-2

Judianne Davis<sup>a,b</sup>, Feng Xu<sup>a,b</sup>, Xiaoyue Zhu<sup>a,b</sup>, William E. Van Nostrand<sup>a,b,\*</sup>

<sup>a</sup> George & Anne Ryan Institute for Neuroscience, University of Rhode Island, Kingston, RI 02881, United States

<sup>b</sup> Department of Biomedical & Pharmaceutical Sciences, University of Rhode Island, Kingston, RI 02881, United States

### ARTICLE INFO

#### Keywords:

Cerebral amyloid angiopathy  
Small vessel disease  
Amyloid  $\beta$  protein  
Dutch mutation  
Transgenic rat  
Microbleed

### ABSTRACT

**Background:** Cerebral amyloid angiopathy (CAA) is common disorder of the elderly, a prominent comorbidity of Alzheimer's disease, and causes vascular cognitive impairment and dementia. Previously, we generated a transgenic rat model of capillary CAA type-1 that develops many pathological features of human disease. However, a complementary rat model of larger vessel CAA type-2 disease has been lacking.

**Methods:** A novel transgenic rat model (rTg-D) was generated that produces human familial CAA Dutch E22Q mutant amyloid  $\beta$ -protein (A $\beta$ ) in brain and develops larger vessel CAA type-2. Quantitative biochemical and pathological analyses were performed to characterize the progression of CAA and associated pathologies in aging rTg-D rats.

**Results:** rTg-D rats begin to accumulate A $\beta$  in brain and develop varying levels of larger vessel CAA type-2, in the absence of capillary CAA type-1, starting around 18 months of age. Larger vessel CAA was mainly composed of the A $\beta$ 40 peptide and most prominent in surface leptomeningeal/pial vessels and arterioles of the cortex and thalamus. Cerebral microbleeds and small vessel occlusions were present mostly in the thalamic region of affected rTg-D rats. In contrast to capillary CAA type-1 the amyloid deposited within the walls of larger vessels of rTg-D rats did not promote perivascular astrocyte and microglial responses or accumulate the A $\beta$  chaperone apolipoprotein E.

**Conclusion:** Although variable in severity, the rTg-D rats specifically develop larger vessel CAA type-2 that reflects many of the pathological features of human disease and provide a new model to investigate the pathogenesis of this condition.

### Introduction

Cerebral amyloid angiopathy (CAA) is a common form of cerebral small vessel disease that is characterized by the accumulation of fibrillar amyloid  $\beta$ -protein (A $\beta$ ) in the cerebral vasculature [1–4]. CAA is a common vascular comorbidity in patients with Alzheimer's disease (AD) but also can occur sporadically affecting >50% of individuals over the age of 80 years [5–8]. Cerebral vascular accumulation of A $\beta$  can result in perivascular neuroinflammation, cerebral infarction, microbleeds, and in severe cases, intracerebral hemorrhages (ICH) [1,3,6,9]. Because of these vascular impacts CAA is a significant cause of vascular-mediated cognitive impairment and dementia (VCID) [4,7,8,10]. Two prominent forms of this condition exist known as CAA type-1 and CAA type-2 [3, 11]. In CAA type-2, fibrillar amyloid accumulates largely within the

vessel wall of meningeal and cortical arterioles [1,3,11]. On the other hand, with CAA type-1 amyloid deposition occurs primarily along capillaries and is present in nearly half of AD cases [3,5,11]. With CAA type-1 fibrillar amyloid deposits engage the surrounding neuropil causing strong perivascular neuroinflammation that is correlated with poorer cognition and dementia in individuals afflicted with AD and in CAA patients [3,5,9,12,13].

As well as the pronounced CAA that is observed in AD patients and sporadic cases of this disease, several familial forms of this condition exist resulting from mutations that reside within the A $\beta$  peptide region of APP gene [14–17]. The first familial CAA mutation identified in A $\beta$  was the Dutch E22Q [14,15]. Dutch CAA patients exhibit early-onset primarily larger vessel CAA type-2 and develop recurrent, and often fatal, ICH [18–20]. Another familial form of CAA is the Iowa D23N A $\beta$  variant

**Abbreviation:** AD, Alzheimer's disease; A $\beta$ , Amyloid  $\beta$ -protein; A $\beta$ PP, Amyloid  $\beta$ -protein precursor; ApoE, Apolipoprotein E; CAA, Cerebral amyloid angiopathy; GFAP, Glial fibrillary acidic protein; Iba-1, Ionized calcium-binding adapter molecule 1; ICH, Intracerebral hemorrhage; VCID, Vascular cognitive impairment and dementia; WT, Wild-type.

\* Corresponding author.

E-mail address: [wvannostrand@uri.edu](mailto:wvannostrand@uri.edu) (W.E. Van Nostrand).

<https://doi.org/10.1016/j.cccb.2022.100133>

Received 28 December 2021; Received in revised form 2 March 2022; Accepted 7 March 2022

Available online 11 March 2022

2666-2450/© 2022 The Authors. Published by Elsevier B.V. This is an open access article under the CC BY-NC-ND license (<http://creativecommons.org/licenses/by-nc-nd/4.0/>).

that occurs adjacent to the site of the Dutch mutation [21]. Although Iowa patients similarly develop early-onset CAA in this case there is a higher predilection for the capillary type-1 form [22–24]. Both Dutch and Iowa CAA can cause VCID in patients [21,25].

Previously, several transgenic mouse lines were developed that express human A $\beta$ PP in brain harboring one or more of the familial CAA mutations [26–28]. Although studies with these earlier CAA transgenic mouse lines have shed light on the role of CAA in small vessel pathology, perivascular neuroinflammation and VCID they have exhibited varying limitations in capturing the full human condition [29–32]. This has prompted the quest to generate better animal models for CAA to more fully understand the pathogenesis of this condition and its role in VCID. To this end, we recently generated a new transgenic rat model for CAA, designated rTg-DI, that produces chimeric Dutch/Iowa CAA mutant A $\beta$  in brain [33]. The rTg-DI rats develop early-onset capillary amyloid deposition that captures many of the pathological features of human CAA type-1 including perivascular neuroinflammation, cerebral microbleeds, small vessel occlusions, white matter degeneration and cognitive deficits [33–36]. However, an analogous rat model for larger vessel CAA type-2 has been lacking. Here we describe the generation and initial characterization a new transgenic rat model of larger vessel CAA type-2 (rTg-D).

## Materials and methods

### Generation of rTg-D transgenic rats

All work with animals was performed in accordance with the United States Public Health Service's Policy on Humane Care and Use of Laboratory Animals and was approved by the University of Rhode Island Institutional Animal Care and Use Committee (AN1718-008). A pcDNA3 vector containing 2.1 kb of human APP (isoform 770) cDNA was used to introduce the mutations Swedish K670N/M671L and Dutch E693Q using the QuikChange kit (Stratagene, La Jolla, CA). The APP770-SwDI cDNA was amplified by PCR using primers containing the NheI 5-linker and SacII 3-linker. The PCR product was digested and subcloned between exons II and IV of a Thy1.2 expression cassette using NheI and SacII restriction sites. The completed construct was entirely sequenced to confirm its integrity. The 9-kb transgene was liberated by NotI/PvuII digestion, purified, and microinjected into pronuclei of Sprague-Dawley single cell embryos. Founder rats were identified by Southern blot analysis of tail DNA. Transgenic offspring were determined by PCR analysis of tail DNA using the following primers specific for human A $\beta$ PP: 5'-CCTGATTGATACCAAGGAAGGCATCCTG-3' and 5'-GTCATCATCGGCTTCTTCTTCCACC-3' (generating a 500-bp product). The rTg-D rats used in this study were maintained as heterozygotes for the transgene and all subsequent breedings were performed with Sprague-Dawley rats. All rats were housed in a controlled room (22  $\pm$  2  $^{\circ}$ C and 40–60% humidity) on a standard 12 h light cycle. Rat chow and water were available *ad libitum*. Both female and male rats were evaluated at each timepoint.

### 2.2. Brain tissue collection and preparation

Rats were euthanized at designated time points and perfused with cold-PBS, forebrains were removed and dissected through the mid-sagittal plane. One hemisphere was fixed with 4% paraformaldehyde overnight at 4  $^{\circ}$ C and subjected to increasing concentrations (10%, 20%, 30%) of sucrose in PBS, then embedded in Optimal Cutting Temperature compound (Sakura Finetek Inc., Torrance, CA, USA) and snap-frozen in dry ice. Sagittal sections were cut at 10  $\mu$ m thickness using a Leica CM1900 cryostat (Leica Microsystems Inc., Bannockburn, IL, USA), placed in a flotation water bath at 40  $^{\circ}$ C, and then mounted on Colorfrost/Plus slides (ThermoFisher Scientific, Houston, TX, USA). The remaining hemispheres were collected, frozen on dry ice and stored at  $-80^{\circ}$ C for ELISA analyses and vascular amyloid isolation.

### 2.3. Immunoblot analysis of human A $\beta$ PP

Forebrain tissues from rTg-D and wild-type (WT) rats were homogenized in 10 vol of 50 mM Tris-HCl (pH 7.5) containing 150 mM NaCl, 1% SDS, 0.5% Nonidet P-40, 5 mM EDTA, and proteinase inhibitor cocktail (Roche Applied Science, Indianapolis, IN). The tissue homogenates were clarified by centrifugation at 14,000  $\times$  g for 10 min. Protein concentrations of the resulting supernatants were determined using the BCA protein assay Kit (Fisher Scientific, Houston, TX). The presence of human A $\beta$ PP in the forebrain tissue homogenates was determined by immunoblotting using monoclonal antibody P2-1, which is specific for human A $\beta$ PP [37]. Bands corresponding to human A $\beta$ PP were visualized using a LICOR imaging system (Lincoln, NE).

### 2.4. ELISA measurements of A $\beta$ peptides

The levels of soluble and insoluble A $\beta$ 40 and A $\beta$ 42 were determined by performing specific ELISAs for each peptide as described [38,39]. Briefly, brain hemispheres were flash frozen and then pulverized in liquid nitrogen. A soluble fraction was obtained by homogenizing brain tissue with 10  $\mu$ L / mg of 1 M sodium carbonate, 500 mM NaCl, pH 11.5 using 0.5 mm zirconium oxide beads in a bullet blender. Aliquots were centrifuged at 1600  $\times$  g at 4  $^{\circ}$ C for 20 min. The supernatant containing the soluble fraction of A $\beta$  was collected. The remaining pellet was suspended in 5 M guanidine-HCl, 50 mM Tris, pH 8.0 and rotated at room temperature for 3 h. Samples were centrifuged and the supernatant was collected, which was the insoluble fraction. For each of the two fractions, a sandwich ELISA was performed. Antibody reagents for the A $\beta$  ELISAs were generously provided by Lilly Research Laboratories, Indianapolis, IN, USA. In the sandwich ELISAs A $\beta$ 40 and A $\beta$ 42 peptides were captured using the carboxyl-terminal specific antibodies m2G3 and m21F12, respectively, and biotinylated m3D6, specific for the N-terminus of human A $\beta$ , was used for detection followed by streptavidin-HRP (Amdex RPN4401V; Fisher Scientific, Pittsburgh, PA, USA). Plates were developed using KPL SureBlue (SeraCare, Milford, MA, USA) and read using a Spectramax M2 plate reader (Molecular Devices, Sunnyvale, CA, USA). Each sample lysate was measured in triplicate and compared to linear standard curves generated with known concentrations of specific human A $\beta$  peptides.

### 2.5. Isolation of cerebral vascular amyloid deposits

Brain vessels were isolated from the cortices of 24 M rTg-D rats as described [26,40]. The isolated cerebral vessels were analyzed microscopically by staining with thioflavin S and immunolabeling with an antibody to collagen IV to confirm the isolation of amyloid-containing vessels. The isolated vessels were treated with 3 mg/ml collagenase at 37  $^{\circ}$ C overnight. The collagenase treated samples were centrifuged at 16,000  $\times$  g for 5 min and the resulting pellet was washed twice with TBS. The amyloid pellet was resuspended in TBS and again analyzed microscopically by staining with thioflavin S and immunolabeling with an antibody to collagen IV to confirm the isolation of vascular amyloid deposits and the absence of vessels.

### 2.6. Immunohistochemical analysis

Antigen retrieval was performed by treating the tissue sections with proteinase K (0.2 mg/ml) for 10 min at 22  $^{\circ}$ C. Primary antibodies were detected with Alexa Fluor 594-conjugated donkey anti-rabbit or Alexa Fluor 488-conjugated goat anti-mouse secondary antibodies (1:1000). Staining for fibrillar amyloid was performed either using Amylo-Glo as described by the manufacturer (Biosensis Inc., Thebarton, South Australia) or staining with thioflavin S. The following antibodies were used for immunohistochemical analysis: mAb66.1 (1:250), which recognizes residues 1–5 of human A $\beta$  [41]; mAb2B4 to detect A $\beta$ 42 (1:1000) and rabbit polyclonal antibody to detect A $\beta$ 40 (1:200;

Biosource, Camarillo, CA) respectively; rabbit polyclonal antibody to collagen type IV to visualize cerebral vessels (1:100; ThermoFisher, Rockford, IL); and rabbit antibodies to NeuN (1:200; cat #MA5-33,103 Invitrogen, Carlsbad, CA), GFAP (1:200; Dako, Santa Clara, CA) and Iba-1 (1:200; Fujifilm Wako Pure Chemical, Osaka, Japan) for detection of neurons, astrocytes and microglia, respectively. ApoE was detected using a rabbit monoclonal antibody (APOE, 1:250, RRID: AB\_2,832,971, Abcam, Cambridge, MA). The presence of osteopontin along occluded/calcified thalamic vessels was detected using a rabbit polyclonal antibody (1:200; cat #ab63856, Abcam) followed by biotinylated anti-rabbit IgG (1:1000; cat #BA-1100, Vector Laboratories, Burlingame, CA) and Vectastain Elite ABC-HRP kit and developed with stable DAB (cat #750,118, Invitrogen). Prussian blue iron staining was performed to detect hemosiderin deposits reflecting signs of previous microhemorrhage [33,42]. Von Kossa calcium staining was used to detect small vessel occlusion/calcifications in the brain [43]. In this case, tissue sections were counterstained with pararosaniline.

## 2.7. Quantitative measures of cerebral vascular pathologies

The percent area amyloid coverage of cerebral vessels, the numbers of cerebral microbleeds and numbers of occluded/calcified vessels in the cortex, hippocampus, thalamus and surface leptomeningeal/pial vessels was determined in rats at each of the specified ages using stereological principles as described [44].

## 2.8. Statistical analysis

Histological and biochemical data were analyzed by *t*-test at the 0.05 significance level.

## Results

### Neuronal expression of human Swedish/Dutch mutant A $\beta$ PP results in accumulation of Dutch mutant A $\beta$ peptides in brain

Previously, we used a neuronal-specific Thy1.2 expression cassette to drive expression human A $\beta$ PP harboring the familial AD Swedish K670N/M671L mutations and the familial CAA Dutch E693Q and Iowa D694N mutations in neurons in the rat brain [33]. This line of rTg-DI rats, that produce chimeric Dutch/Iowa CAA mutant A $\beta$  peptides, develops early-onset and progressive capillary CAA type-1 and associated vasculopathies [33,34,36]. Since the Dutch E693Q mutation in the APP gene results in primarily larger vessel CAA type-2 in patients [18–20] we reasoned that producing Dutch E22Q mutant A $\beta$  in the brains of rats would similarly lead to CAA type-2 pathology. To test this, the neuronal-specific Thy1.2 expression cassette, similar to the one utilized to produce rTg-DI rats, was again used to drive expression human A $\beta$ PP in neurons in the rat brain harboring the familial AD Swedish K670N / M671L mutations and now the sole the familial CAA Dutch E693Q mutation. The Swedish A $\beta$ PP mutations were again incorporated into the transgene solely to enhance  $\beta$ -secretase processing and production of A $\beta$  peptides [45]. The familial CAA Dutch mutation was included in the transgene to yield Dutch CAA mutant E22Q A $\beta$  peptides in brain which exhibit markedly enhanced fibrillogenic and vascular pathogenic properties compared to non-mutated A $\beta$  [46,47]. These transgenic rats (rTg-D) were generated by microinjection of the human APP770-SwD construct into oocytes in a Sprague-Dawley background. The presence of the human A $\beta$ PP transgene was validated in founder and subsequent offspring rats by PCR analysis. All rTg-D rats used in the subsequent characterization experiments presented below were heterozygous for the human A $\beta$ PP transgene.

The rTg-D rats at 3 months (M) of age were evaluated for expression of the human A $\beta$ PP transgene using the human A $\beta$ PP-specific monoclonal antibody P2-1 [37]. Immunofluorescence labeling presented in Fig. 1A-F shows that neuronal human A $\beta$ PP expression was detected

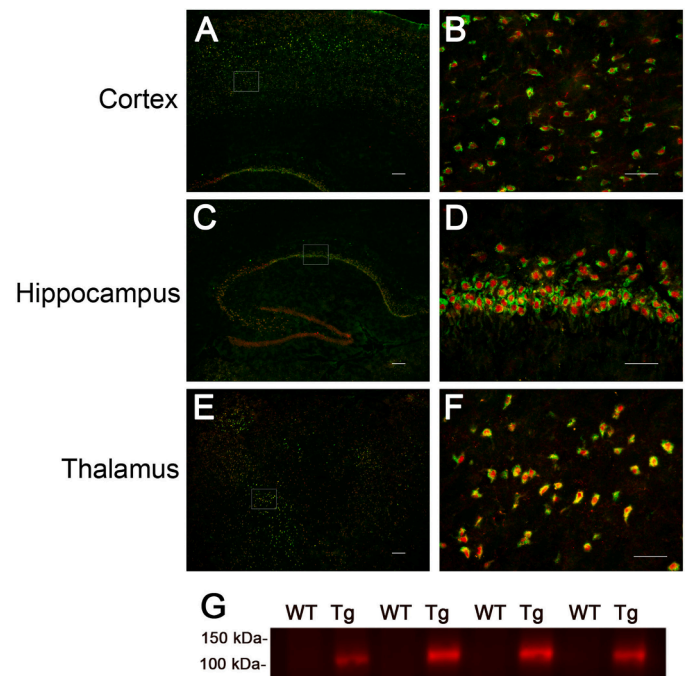


**Fig. 1.** Analysis of transgenic human A $\beta$ PP expression in rTg-D rats. Brain sections from 3 M old rTg-D rats were immunolabeled with the mouse monoclonal antibody mAbP2-1 to specifically detect human A $\beta$ PP (green) and the rabbit polyclonal antibody NeuN to detect neurons (red). Transgene-encoded human A $\beta$ PP expression was detected in neurons in cortex (A), hippocampus (C) and thalamus (E). Scale bars = 10  $\mu$ m. Higher magnification images of the boxed regions show human A $\beta$ PP expression in neurons of the motor cortex (B), CA1 region of the hippocampus (D) and the ventrolateral thalamic nucleus (F). Scale bars = 50  $\mu$ m. (G) Immunoblot analysis of human A $\beta$ PP expression in total brain homogenates from wild-type rats and rTg-D rats. (For interpretation of the references to color in this figure legend, the reader is referred to the web version of this article.)

throughout the cortex, hippocampus and thalamus, similar to the expression pattern we previously documented in rTg-DI rats [33]. Immunoblot analysis using mAbP2-1 confirmed that human A $\beta$ PP transgene expressed protein was observed in rTg-D rats (Fig. 1G).

The accumulation of human Dutch mutant A $\beta$  peptides was measured by ELISA in rTg-D brains as they aged from 6 to 24 M. At 6 M of age no appreciable accumulation of soluble or insoluble A $\beta$ 40 or A $\beta$ 42 was detected (data not shown). However, as the rTg-D rats aged from 12 to 24 M there was a progressive increase in the amounts of both soluble A $\beta$ 40 and A $\beta$ 42 in brain (Fig. 2A). The shorter A $\beta$ 40 isoform comprised >95% of this soluble pool of A $\beta$ . Similarly, there was a progressive robust accumulation of both insoluble A $\beta$ 40 and A $\beta$ 42 as the rats aged, where again the vast majority of accumulated insoluble A $\beta$  peptide was the shorter A $\beta$ 40 isoform (Fig. 2B). Although cerebral A $\beta$  accumulates in the aging rTg-D rats the extent of the accumulation varied widely between some individual rats. These results show that expression of the human Swedish/Dutch mutant human A $\beta$ PP transgene in neurons in rTg-D rats results in accumulation of primarily A $\beta$ 40 in brain starting at  $\approx$ 12 M of age.

### Accumulation of parenchymal A $\beta$ and cerebral vascular amyloid in aging rTg-D rats

Because the levels of insoluble A $\beta$ 40 begin to increase at 12 M and with further aging in the brains of rTg-D rats we next investigated for the accumulation and location of A $\beta$ . Diffuse parenchymal deposits of A $\beta$  first appeared primarily in the cortex at 12 M of age and increased as the rTg-D rats aged to 24 M (Fig. 3). These A $\beta$  deposits did not stain with

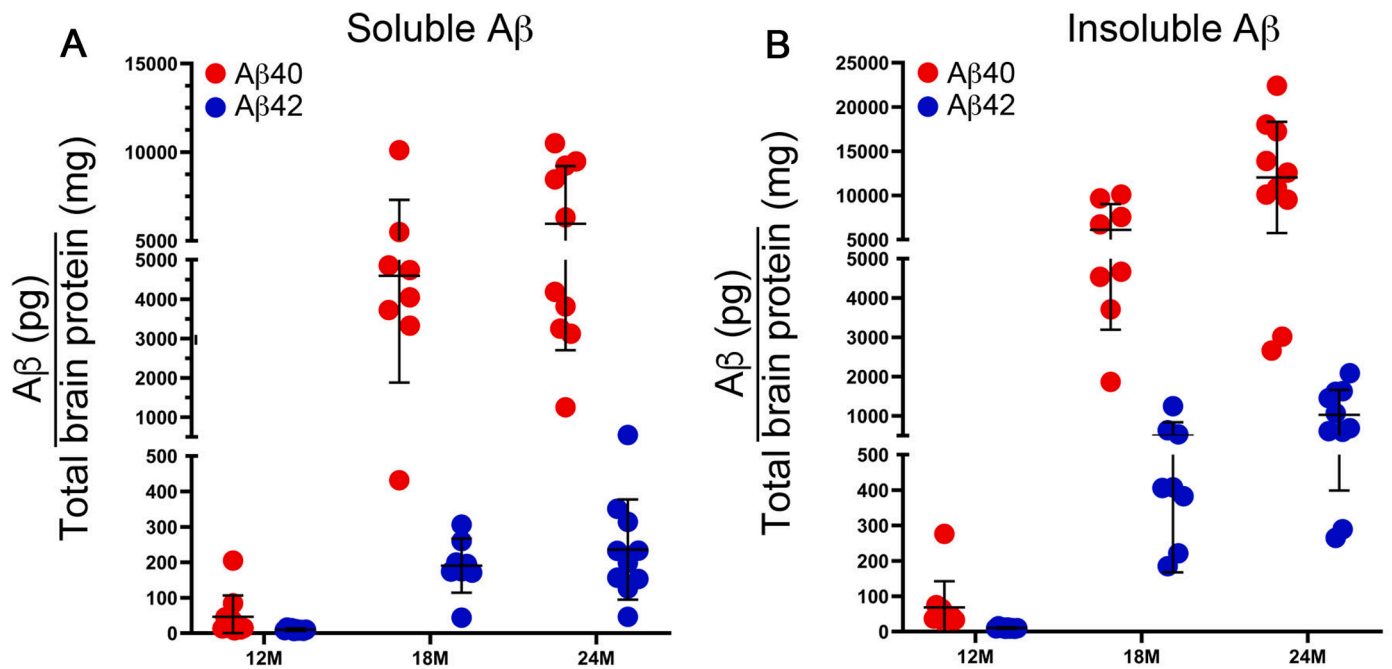


**Fig. 2.** Progressive accumulation of A $\beta$  peptides in rTg-D rats. The levels of soluble (A) and insoluble (B) A $\beta$ 40 (red) and A $\beta$ 42 (blue) peptides in the forebrains of rTg-D rats at designated ages were measured by ELISA as described in “Material and methods.” The data presented are the means  $\pm$  S.D. of triplicate measurements in 8–10 rTg-D rats per group. (For interpretation of the references to color in this figure legend, the reader is referred to the web version of this article.)

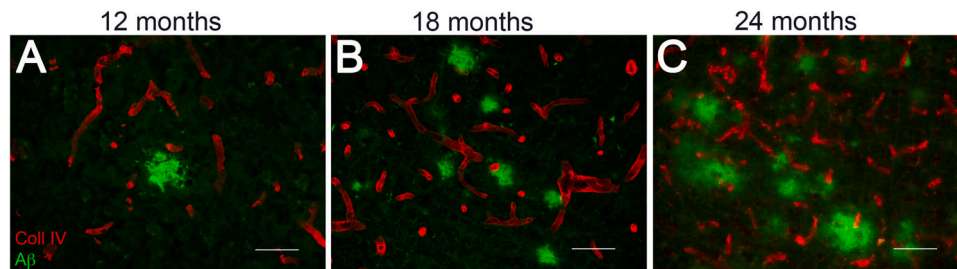


**Fig. 3.** Accumulation of diffuse parenchymal A $\beta$  deposits in rTg-D rats. Brain sections from 12 to 24 M old rTg-D rats were immunolabeled for A $\beta$  (green) and for collagen type IV to identify cerebral vessels (red). Representative images show diffuse parenchymal A $\beta$  deposits in the cortex of 12 M (A), 18 M (B) and 24 M (C) rTg-D rats. Scale bars = 50  $\mu$ m. (For interpretation of the references to color in this figure legend, the reader is referred to the web version of this article.)

thioflavin S or Congo red indicating their non-fibrillar state (data not shown). We next investigated for the presence and location of fibrillar amyloid deposits by staining with thioflavin S. In 18–24 M rTg-D rats there was evidence of prominent fibrillar amyloid in the larger vessels of the cortex (Fig. 4A,D) and thalamus (Fig. 3B,E). Further, there were animals that exhibited robust amyloid deposition in surface leptomeningeal/pial vessels and penetrating arterioles (Fig. 4C,F), all reminiscent of CAA type-2. CAA affected vessels in these brain regions of rTg-D rats generally ranged in size from  $\approx$ 15–200  $\mu$ m in diameter. Quantitation of the larger vessel CAA load at 12 M, an age with little or no accumulation of insoluble A $\beta$  (Fig. 2B), showed no appreciable evidence of vascular amyloid in any brain region of the rats (Fig. 4G-I). On the other hand, once the rTg-D rats aged to 18 M many of them now showed vascular amyloid with mean larger vessel CAA coverage loads ranging from 3 to 5%. However, it was noted that some rats still exhibited little evidence of CAA at this age in any region. As the rTg-D rats aged further to 24 M the vascular amyloid coverage generally increased but again there was a wide range in the extent of vascular amyloid with some animals still showing little CAA. At 24 M the surface leptomeningeal/pial vessels and penetrating arterioles showed the most consistent and robust CAA with some rats presenting with  $\geq$ 40% of vessel area covered in amyloid (Fig. 4I).

Our previous transgenic rat CAA model rTg-DI develops early-onset and robust accumulation of vascular amyloid almost exclusively on capillaries with vessel diameters of  $\leq$ 10  $\mu$ m, which is characteristic of CAA type-1 (Fig. 5A-C). Notably, despite the emergence of larger vessel CAA type-2 there was striking lack of amyloid accumulation on the capillaries of rTg-D rats (Fig. 5D-F). This marked difference in CAA pathology between rTg-D rats and rTg-DI rats indicates that the respective Dutch E22Q mutant A $\beta$  and chimeric Dutch E22Q / Iowa D23N mutant A $\beta$  peptides target very different cerebral vascular beds in the rats.

Immunofluorescence labeling with isoform-specific antibodies revealed that the major component of vascular amyloid was the shorter A $\beta$ 40 (Fig. 6A-C). In support of this, ELISA analysis of vascular amyloid isolated from cerebral vessels prepared from rTg-D rats confirmed that nearly  $\approx$ 95% of the vascular amyloid was comprised of A $\beta$ 40 peptide (Fig. 6D-F). Taken together, these data show that after 12 M of age rTg-D rats specifically develop progressive larger vessel CAA type-2 primarily composed of A $\beta$ 40, but the extent of CAA can vary widely between animals.

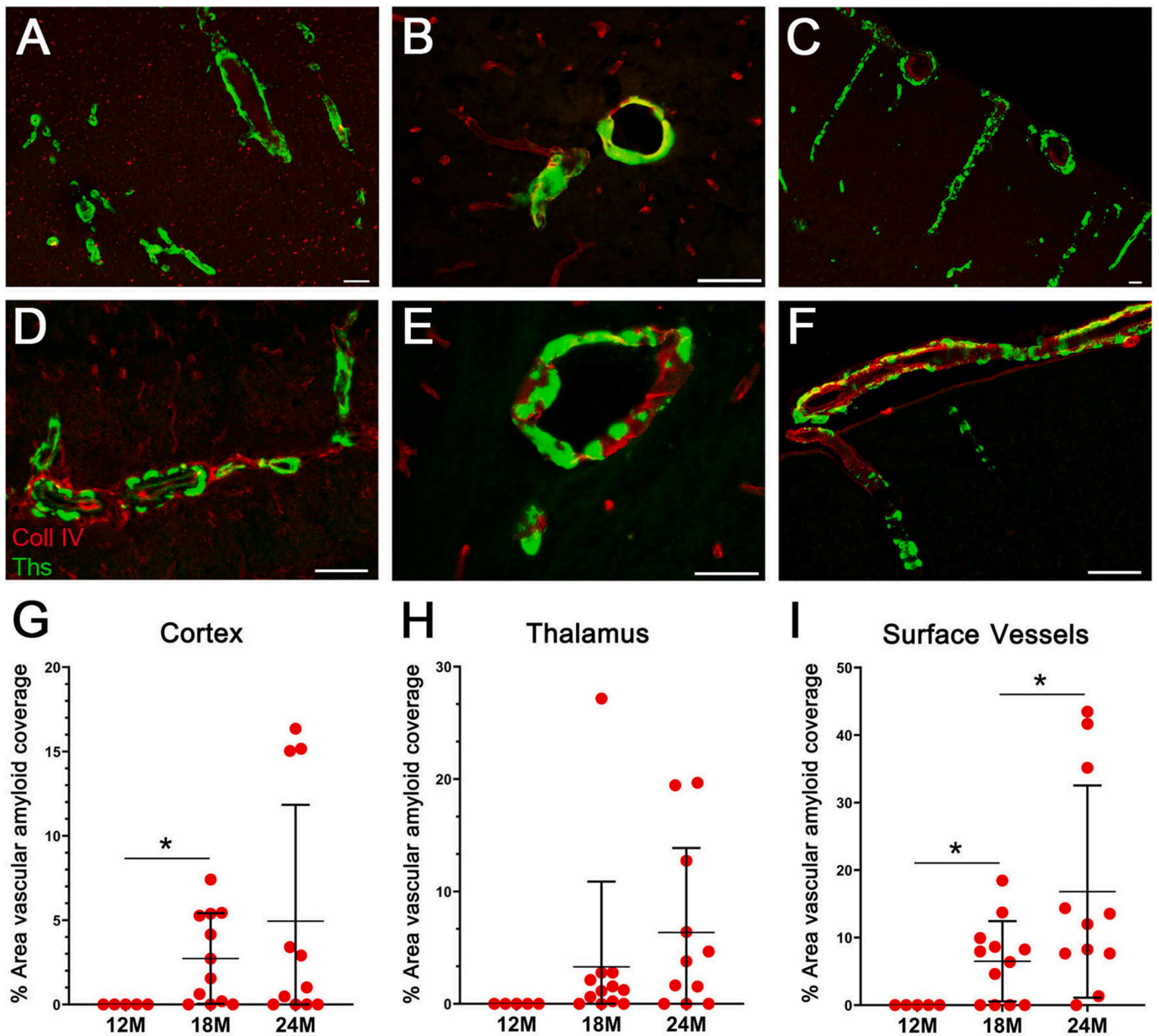


**Fig. 4.** Progressive accumulation of CAA type-2 in rTg-D rats. Brain sections from 24 M old rTg-D rats were stained for fibrillar amyloid using thioflavin-S (green) and immunolabeled for collagen type IV to identify cerebral vessels (red). Representative images show accumulation of amyloid in larger vessels in the cortex (A,D), thalamus (B,E) and surface leptomeningeal/pial vessels and penetrating arterioles (C,F). Scale bars = 50  $\mu$ M. Quantitation of vascular thioflavin-S positive amyloid load at 12, 18 and 24 M of age in the cortex (G), thalamus (H) and surface leptomeningeal/pial vessels (I). Data shown are mean  $\pm$  S.D. of 6–11 rTg-D rats per group; \* $p < 0.05$ . (For interpretation of the references to color in this figure legend, the reader is referred to the web version of this article.)

### 3.3. Accumulation of vascular amyloid promotes cerebral microbleeds and small vessel occlusions in rTg-D rats

Cerebral microbleeds are a prominent clinical manifestation of CAA in patients [1–3,9]. We next investigated the presence of cerebral microbleeds in a subset of 24 M rTg-D rats that presented with higher CAA loads by performing staining for perivascular hemosiderin. Representative images of microbleeds found in the cortex, hippocampus, thalamus and surface pial vessels are shown in Fig. 7A–D. Quantitation of the number of microbleeds showed that they were generally scarce in the cortex and hippocampus but more abundant in the thalamus and surface leptomeningeal/pial vessels (Fig. 7E).

Occlusion and calcification of cerebral vessels are other vascular manifestations reported in sporadic and familial CAA patients and observed in our previous rTg-DI model for CAA type-1 [9,24,48,49].

Calcium staining of rTg-D brain tissue sections revealed calcified vessel occlusions that were restricted to the thalamus (Fig. 8A,B), the same brain region that uniquely exhibited these lesions in rTg-DI rats [33]. The number of thalamic small vessel occlusions were counted in rTg-D rats at 24 M of age showing that most, but not all, animals exhibited these lesions (Fig. 8C). It was previously reported that osteopontin, a factor that promotes calcification, was associated with vessel calcifications in Dutch-type CAA patients [50]. Similarly, we found osteopontin labeled vessel calcifications in rTg-D rats (Fig. 8E).

### Accumulation of larger vessel amyloid in rTg-D rats does not promote perivascular glial cell responses

Previously, we showed that accumulation of capillary amyloid in rTg-DI rats, a model of CAA type-1 where the amyloid is engaged with

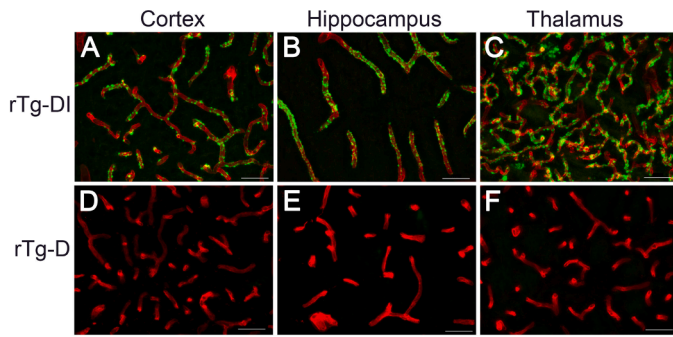


**Fig. 5.** rTg-D rats do not accumulate CAA type-1 capillary amyloid. Brain sections from 12 M old rTg-DI rats (A-C) and 24 M old rTg-D rats (D-F) were stained for fibrillar amyloid using thioflavin-S (green) and immunolabeled for collagen type IV to identify cerebral vessels (red). Representative images show abundant capillary amyloid in the cortex, hippocampus and thalamus of rTg-DI rats but absent in rTg-D rats. Scale bars = 50 μm. (For interpretation of the references to color in this figure legend, the reader is referred to the web version of this article.)

the surrounding parenchyma, triggers the activation and proliferation of perivascular glial cells [33,34]. However, in the present rTg-D rats, a model of CAA type-2, the vascular amyloid is sheathed within the larger vessel wall and generally lacks parenchymal involvement. Therefore, we next determined if CAA type-2 vascular amyloid deposits in rTg-D rats enhanced perivascular glial cell responses. In the presence of rTg-D larger vessel CAA the astrocyte numbers and morphology appeared similar to WT rats which lack vascular amyloid (Fig. 9C,A; respectively). On the other hand, rTg-DI rats which exhibit capillary amyloid stimulated a robust increase and activation of astrocytes (Fig. 9E).

Likewise, we found that CAA type-2 in the rTg-D rats did not stimulate perivascular microglia, rather they maintained their normal numbers and resting state with numerous, extended processes similar to WT rats (Fig. 9D,B; respectively). In contrast, capillary amyloid in the rTg-DI CAA type-1 rats caused highly elevated numbers and activation of perivascular microglia (Fig. 9F). Together, these findings show that the vascular amyloid in larger vessel CAA type-2 in rTg-D rats does promote perivascular glial inflammatory responses, likely due to its inaccessibility to surrounding brain parenchyma.

*The amyloid chaperone ApoE does not accumulate on larger vessel amyloid in rTg-D rats*

ApoE, largely produced by astrocytes and microglia in the brain parenchyma, is a well-recognized binding chaperone of Aβ that can influence the development of AD and CAA [51–53]. Furthermore, ApoE can strongly bind Aβ aggregates, inhibit Aβ fibril formation and co-localize with fibrillar amyloid deposits [54–58]. We determined if ApoE co-localizes with CAA type-2 fibrillar amyloid deposits in rTg-D rats. Fig. 10C,D shows that larger vessel fibrillar amyloid in the cortex and thalamus, respectively, of rTg-D rats did not show any appreciable immunolabeling for ApoE. In contrast, vascular amyloid deposits on the capillaries of rTg-DI rats, which are exposed to ApoE-producing astrocytes and microglia in the surrounding brain parenchyma, are strongly immunolabeled for ApoE. These findings further support that CAA type-2 larger vessel amyloid in the rTg-D rats is sequestered within the vessel walls and has little, if any, exposure to the adjacent brain parenchyma in the absence of dyschorric amyloid.

**Discussion**

Despite the significance of CAA in the growing elderly population

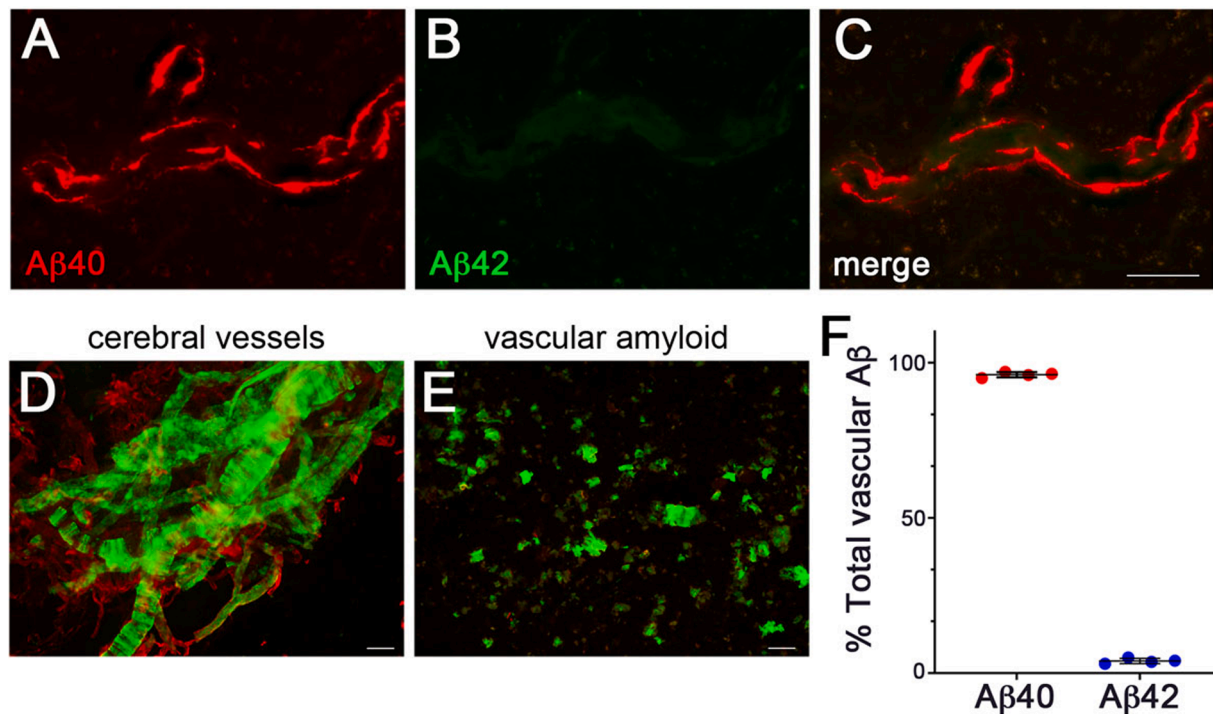


**Fig. 6.** Aβ composition of cerebral vascular Aβ deposits in rTg-D Rats. Brain sections from rTg-D rats at 24 M of age were immunolabeled with an antibody specific for Aβ40 (red) (A) and an antibody specific for Aβ42 (green) (B) and merged (C). Representative images are from the cortex. Scale bar = 50 μm. (D) Cerebral vessels were isolated from 24 M old rTg-D rats and stained with thioflavin-S to visualize fibrillar amyloid deposits (green) and immunolabeled with an antibody to collagen IV to view the cerebral vessels (red). Scale bar = 50 μm. (E) Cerebral vascular amyloid deposits after digestion and removal of the vessels and stained for fibrillar amyloid using thioflavin S (green). Scale bar = 50 μm. (F) ELISA measurements were performed to determine the amounts of Aβ40 and Aβ42 in the vascular amyloid deposits prepared from the cerebral vessels isolated from rTg-D rat brain. Data shown are mean ± S.D. of 4 rTg-D rats. (For interpretation of the references to color in this figure legend, the reader is referred to the web version of this article.)

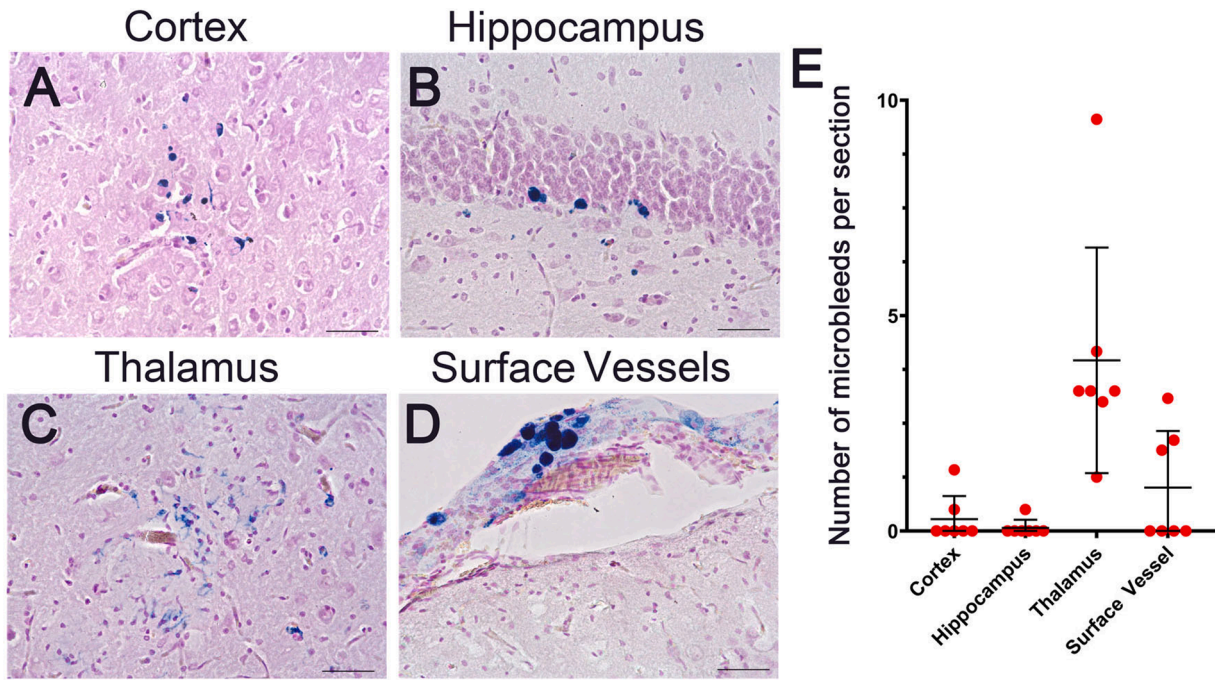


**Fig. 7.** Cerebral microbleeds in rTg-D rats. Brain sections from 24 M old rTg-D rats were stained for hemosiderin to identify the presence of microbleeds (blue). Representative images from the cortex (A), hippocampus (B), thalamus (C), and surface vessels (D). Scale bars = 50  $\mu$ m. (E) The number of microbleeds were counted in the different brain regions. Data represent the mean  $\pm$  S.D. 7 rTg-D rats. (For interpretation of the references to color in this figure legend, the reader is referred to the web version of this article.)

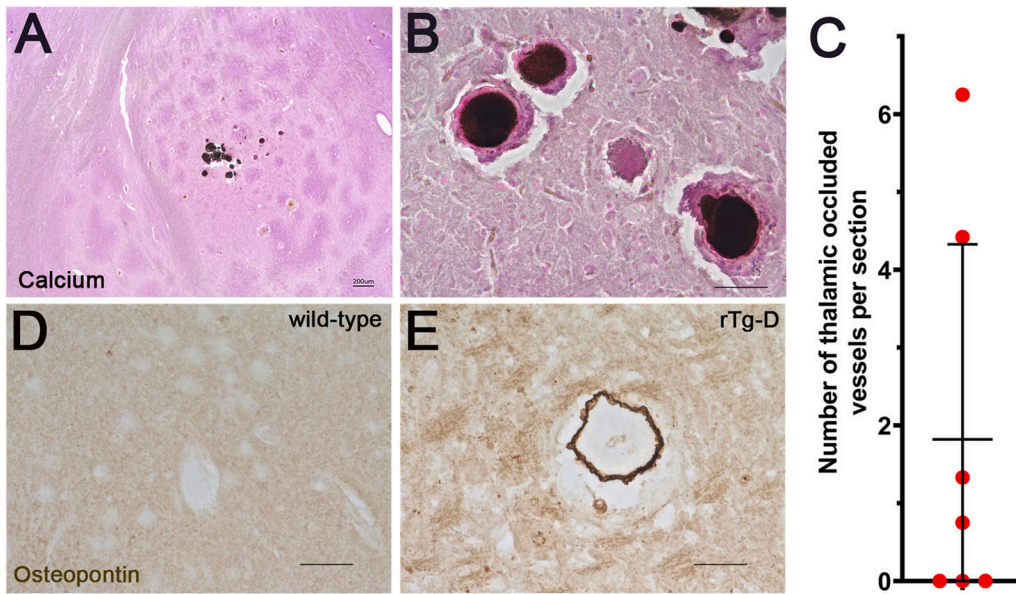


**Fig. 8.** Cerebral vessel occlusions in rTg-D rats. Brain sections from 24 M old rTg-D rats were stained for calcium (black) and counterstained with pararosaniline (pink). Representative images from the thalamic region (A,B). (A) scale bar = 200  $\mu$ m. (B) scale bar = 50  $\mu$ m. The number of thalamic small vessel occlusions were counted in 24 M old rTg-D rats (C). Data represent the mean  $\pm$  S.D. of 7 rTg-D rats. Brain sections from 24 months old wild-type and rTg-D rats were stained for osteopontin (brown). Representative images from the thalamic region of a wild-type rat (D) and rTg-D rat (E). Scale bars = 50  $\mu$ m. (For interpretation of the references to color in this figure legend, the reader is referred to the web version of this article.)

our current understanding of the pathogenesis remains limited and there are no effective treatments. For over two decades now the scientific field has largely relied on transgenic mouse lines to investigate this disease [26–28,59–61]. However, transgenic mice develop varying levels of CAA and, in most models, in the presence of AD parenchymal amyloid pathologies. Thus, there remains a need for better experimental models that more faithfully mimic CAA in humans to study the development of disease and downstream consequences of vascular amyloid pathology. To this end, we previously reported on the generation and characterization of a novel transgenic rat line rTg-DI that specifically develops CAA type-1 [33]. The rTg-DI rats were designed to express human A $\beta$ PP

in neurons within the brain harboring the chimeric Dutch E693Q / Iowa D694N familial CAA mutations. We showed that rTg-DI develop early-onset and progressive capillary CAA accompanied by a strong perivascular neuroinflammatory response, pericyte loss, cerebral microbleeds, small vessel occlusions, progressive white matter degeneration and cognitive impairment [33,34,36]. The pathologies that emerge in rTg-DI rats reflect many of the pathological features of CAA type-1 in humans. However, they do not inform on the pathogenesis of larger vessel CAA type-2.

The presence of the chimeric Dutch E22Q / Iowa D23N CAA mutant A $\beta$  peptide in rTg-DI rats reflects more the pathology of familial Iowa

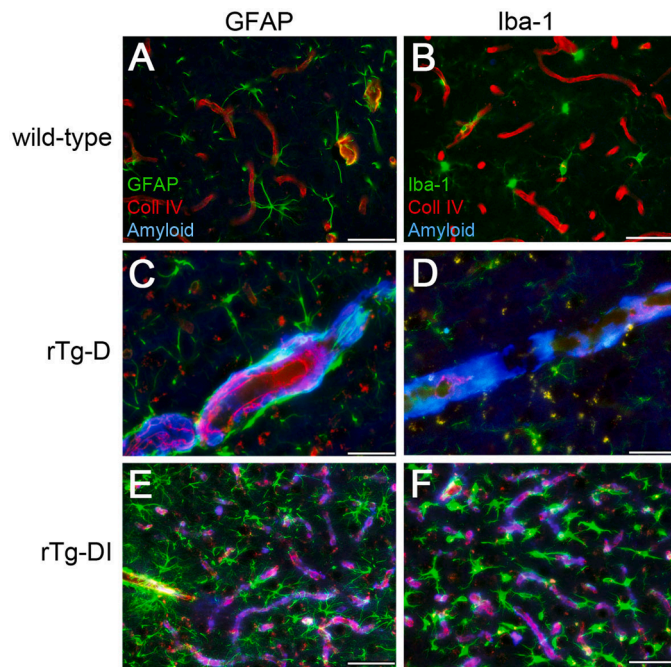


**Fig. 9.** Comparison of perivascular glial activation in the cortex of rTg-D CAA type-2 rats and rTg-DI CAA type-1 rats. Brain sections from 12 M WT rats (A,B), 18 M rTg-D rats (C,D) and 12 M rTg-DI rats (E,F) were stained for fibrillar amyloid (blue), immunolabeled with an antibody to collagen IV to identify cerebral microvessels (red) and immunolabeled with an antibody to GFAP to identify astrocytes (green) (A,C,E) or immunolabeled with an antibody to Iba-1 to identify microglia (green) (B,D,F). Scale bars = 50  $\mu$ m. rTg-D CAA type-2 rats do not show increased numbers and activation of perivascular astrocytes and microglia, similar to WT rats. In contrast, rTg-DI CAA type-1 rats exhibit strong increases in perivascular reactive astrocytes and activated microglia in response to the prominent cerebral capillary amyloid. (For interpretation of the references to color in this figure legend, the reader is referred to the web version of this article.)

CAA that can strongly affect capillaries [21,22,24]. On the other hand, the presence of Dutch E22Q mutation in patients causes primarily larger vessel CAA type-2 [16,18–20]. Therefore, we reasoned that incorporating just the Dutch CAA A $\beta$  mutation in the human A $\beta$ PP transgene would lead to a preference for CAA type-2. Indeed, we found that rTg-D rats appear to only develop larger vessel CAA type-2 in the absence of capillary CAA type-1 (Figs. 4 and 5). Although the neuronal expression pattern of the respective human A $\beta$ PP transgenes was similar between rTg-D rats and rTg-DI rats the time line for the emergence of larger vessel CAA type-2 in rTg-D rats (>12 M) was markedly prolonged compared with appearance of CAA type-1 capillary amyloid in rTg-DI rats ( $\approx$ 3 M) [33, 34]. Previously, we showed that chimeric Dutch E22Q / Iowa D23N CAA mutant A $\beta$  assembles into amyloid fibrils much more rapidly than the single Dutch E22Q CAA mutant A $\beta$  peptide [47]. This difference in fibril assembly kinetics could explain the more rapid development of CAA in rTg-DI rats compared to rTg-D rats. This difference could also explain why rTg-DI rats preferentially develop capillary CAA type-1 whereas rTg-D rats develop larger vessel CAA type-2. In the case of rTg-DI rats, neuronally-derived chimeric Dutch E22Q / Iowa D23N mutant A $\beta$  may migrate to the capillary bed where it is less efficiently cleared across the blood-brain barrier allowing it to congregate, rapidly assemble and deposit [62]. On the other hand, in rTg-D rats neuronally-derived Dutch E22Q mutant A $\beta$  could similarly migrate to the capillary bed where it remains more soluble due to its slower assembly kinetics allowing it to travel along intramural periarial drainage clearance routes to larger vessels where it eventually assembles and deposits as amyloid fibrils [63,64]. Regardless of the reason, the present findings clearly show that Dutch E22Q mutant A $\beta$  causes CAA

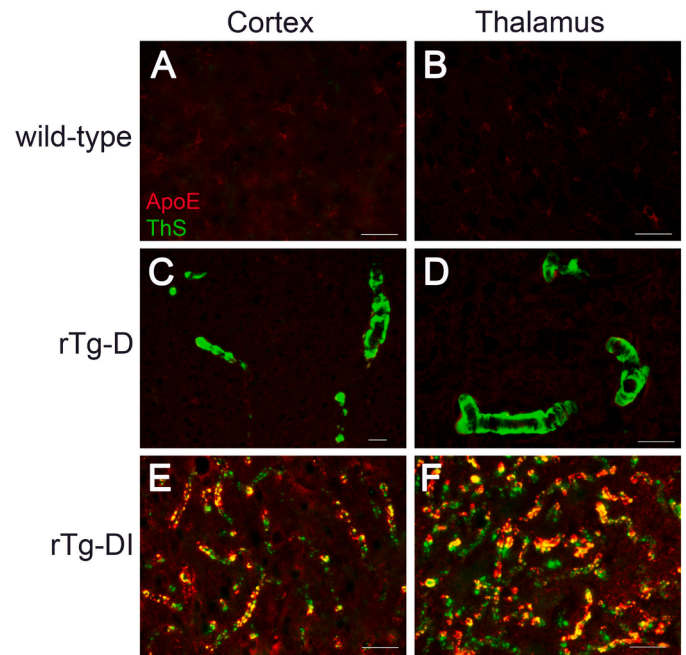


**Fig. 10.** ApoE does not co-localize with vascular amyloid in rTg-D CAA type-2 rats. Brain sections from 12 M wild-type rats (A,B), 18 M rTg-D rats (C,D) and 12 M rTg-DI rats (E,F) were stained for fibrillar amyloid using thioflavin-S (green), immunolabeled with an antibody to apoE (red). Scale bars = 50  $\mu$ m. ApoE exhibited little, if any, co-localization with larger vessel amyloid deposits in the cortex or thalamus of rTg-D CAA type 2 rats. In contrast, ApoE strongly co-localized with capillary amyloid deposits in the cortex and thalamus of rTg-DI CAA type-1 rats. (For interpretation of the references to color in this figure legend, the reader is referred to the web version of this article.)

type-2 in rats whereas the chimeric Dutch E22Q / Iowa D23N mutant A $\beta$  leads to a strong preference for capillary CAA type-1.

In addition to the present rTg-D rats exhibiting a delayed onset of CAA formation compared to rTg-DI rats the extent of CAA type-2 was somewhat variable. Some animals showed appreciable larger vessel CAA at 18 M, especially in the cortex and surface leptomeningeal/pial vessels, whereas other did not (Fig. 4). As the rTg-D rats aged to 24 M more animals exhibited CAA, but some still revealed a paucity of vascular amyloid. This was not related to sex differences as some male and female rats showed CAA at  $\approx$ 18 M whereas others of both sexes showed little CAA even at 24 M. We did not observe differential expression of the human A $\beta$ PP transgene that could account for the variability in CAA presentation. Perhaps since the CAA is still emerging at 18–24 M it is possible that if the rTg-D rats aged further than 24 M the CAA pathology would become more robust and uniform. Indeed, some mouse A $\beta$ PP transgenic lines are variable in amyloid pathology at earlier stages and become more consistent with aging [65]. Furthermore, previously reported Dutch mutant A $\beta$  transgenic mice were even slower in CAA development than rTg-D rats and did not present with vascular amyloid pathology until after 24 M of age [27]. In any case, once the vascular amyloid pathology emerges in rTg-D rats it can become severe in affected vessels.

The accumulation of vascular amyloid in Dutch CAA patients and Iowa CAA patients leads to VCID [21,25]. Similarly, we previously found that robust CAA type-1 pathology in rTg-DI rats also causes cognitive impairments characterized by a ‘cognitive slowing’ effect [33,35]. In contrast, analysis of a cohort of rTg-D rats up to 15 M of age failed to reveal any deficits in a battery of behavioral tests (data not shown). However, subsequent pathological analyses showed that rTg-D rats have minimal, if any, accumulation of cerebral A $\beta$  or CAA formation at this age. Thus, any emerging cognitive deficits in rTg-D rats would likely not be evident until 24 M or older when more significant CAA and associated

vessel pathology is evident and needs future examination.

Severe cases of CAA, particularly in Dutch CAA patients, exhibit recurrent and often fatal ICH resulting from extensive vascular amyloid accumulation [18–20]. At 24 M of age some rTg-D rats exhibited microbleeds and vessel occlusions (Figs. 7 and 8). Although some microhemorrhages were observed in the surface leptomeningeal/pial vessels the presence of microbleeds and vessel occlusions were most abundant in the thalamic region. Osteopontin, a secreted phosphoprotein that is induced by TGF- $\beta$ 1, promotes vessel calcifications in a variety of diseases including atherosclerosis, diabetes mellitus and chronic renal failure [66,67]. It was previously shown that osteopontin co-localizes with vessel calcifications in Dutch-type CAA [50]. The co-localization of osteopontin with thalamic vessel calcifications in rTg-D rats further demonstrates the consistency of the model with human disease. Interestingly, the same types of thrombotic events were found largely restricted to the thalamic region in rTg-DI rats with extensive capillary amyloid [33,36]. It is unclear why both rTg-D rats with CAA type-2 and rTg-DI rats with CAA type-1 would produce microbleeds and vessel occlusions primarily in the thalamus. Perhaps this is due to some difference in blood vessels in the thalamic region or some unique anatomical feature of the rat brain. Alternatively, it is a consequence of driving transgene human A $\beta$ PP expression with the same Thy1 promoter in a similar set of neurons. Further aging of rTg-D rats and more progression of larger vessel CAA may begin to alter this unique pattern of thrombotic events and lead to their emergence in other brain regions.

Perivascular neuroinflammatory responses are strikingly different between CAA type-1 and CAA type-2 [3,11–13]. In CAA type-1, the fibrillar amyloid adheres to the abluminal side of the brain capillaries and is in contact with the adjacent brain neuropil. This provides direct interaction between the deposited amyloid fibrils and perivascular astrocytes and microglia leading to proliferation and activation of these cells [3,12,13]. This is faithfully reflected in rTg-DI CAA type-1 rats where the deposited capillary amyloid robustly activates perivascular astrocytes and microglia producing a strong inflammatory signature [33,34]. In contrast, in CAA type-2 the fibrillar amyloid is deposited within the larger vessel wall in the smooth muscle cell medial layer [1, 3]. In the absence of vessel disruption these amyloid fibrils are sequestered within the vessel wall and have no direct contact with the surrounding neuropil, thus do not stimulate perivascular glial cells. Indeed, we observed that the CAA type-2 that forms in rTg-D rats does not promote perivascular astrocytes or microglia (Fig. 9). This confinement of vascular amyloid fibrils in rTg-D CAA type-2 rats was further supported by the finding that A $\beta$  chaperone ApoE, which is largely produced by astrocytes and microglia in the brain, did not co-localize with vascular amyloid in this model. In contrast, in the rTg-DI rats the capillary amyloid fibrils have direct contact with the neuropil and strongly accumulate ApoE [56].

Although the present findings show that the novel rTg-D rats recapitulate many of the pathological features of human CAA type-2 and are distinct from rTg-DI capillary CAA type-1 rats presently there are several limitations with this model. First, up to 24 M of age the extent of larger vessel CAA is somewhat variable. Although specific vessels that have CAA can be affected heavily there are numerous vessels that do not present with vascular amyloid. As mentioned above, with further aging the extent of larger vessel CAA may increase. Alternatively, maybe only a subset of vessels is susceptible to accumulating fibrillar amyloid in this model. Second, cerebral microbleeds and vessel occlusions also tended to be variable, although this may also be dependent on further aging of this model. Lastly, cognitive deficits were not observed in rTg-D rats up to 15 M of age. However, pathology at this age was minimal. With further aging and development of more severe vascular amyloid pathology it is possible that cognitive deficits would emerge. Future studies focused at further aging of rTg-D rats should address these points. Despite these limitations in rTg-D rats this unique model provides new opportunities to investigate the pathogenic development of larger vessel CAA type-2 and its relation of VCID in a species that is more amenable to

neuroimaging and cognitive testing. Additionally, rTg-D rats provide a new platform for the development of biomarkers and preclinical testing of therapeutic interventions for CAA type-2.

## Declaration of Competing Interests

None.

## Acknowledgements

This research was funded in part by the National Institutes of Health grant number RO1NS092696. Antibody reagents for the A $\beta$  ELISAs were generously provided by Lilly Research Laboratories, Indianapolis, IN.

## References

- [1] A.A. Rensink, et al., Pathogenesis of cerebral amyloid angiopathy, *Brain Res. Brain Res. Rev.* 43 (2) (2003) 207–223.
- [2] A. Viswanathan, S.M. Greenberg, Cerebral amyloid angiopathy in the elderly, *Ann. Neurol.* 70 (6) (2011) 871–880.
- [3] J. Attems, et al., Review: sporadic cerebral amyloid angiopathy, *Neuropathol. Appl. Neurobiol.* 37 (1) (2011) 75–93.
- [4] G. Banerjee, et al., The increasing impact of cerebral amyloid angiopathy: essential new insights for clinical practice, *J. Neurol. Neurosurg. Psychiatry* 88 (11) (2017) 982–994.
- [5] K.A. Jellinger, Alzheimer disease and cerebrovascular pathology: an update, *J. Neural. Transm. (Vienna)* 109 (5–6) (2002) 813–836.
- [6] A. Biffi, S.M. Greenberg, Cerebral amyloid angiopathy: a systematic review, *J. Clin. Neurol.* 7 (1) (2011) 1–9.
- [7] Z. Arvanitakis, et al., Cerebral amyloid angiopathy pathology and cognitive domains in older persons, *Ann. Neurol.* 69 (2) (2011) 320–327.
- [8] P.A. Boyle, et al., Cerebral amyloid angiopathy and cognitive outcomes in community-based older persons, *Neurology* 85 (22) (2015) 1930–1936.
- [9] E. Auriel, S.M. Greenberg, The pathophysiology and clinical presentation of cerebral amyloid angiopathy, *Curr. Atheroscler. Rep.* 14 (4) (2012) 343–350.
- [10] S.M. Greenberg, et al., Amyloid angiopathy-related vascular cognitive impairment, *Stroke* 35 (2004) 2616–2619, 11 Suppl 1.
- [11] D.R. Thal, et al., Two types of sporadic cerebral amyloid angiopathy, *J. Neuropathol. Exp. Neurol.* 61 (3) (2002) 282–293.
- [12] A.J. Rozemuller, W.A. van Gool, P. Eikelenboom, The neuroinflammatory response in plaques and amyloid angiopathy in Alzheimer's disease: therapeutic implications, *Curr. Drug Targets CNS Neurol. Disord.* 4 (3) (2005) 223–233.
- [13] E. Richard, et al., Characteristics of dyschoric capillary cerebral amyloid angiopathy, *J. Neuropathol. Exp. Neurol.* 69 (11) (2010) 1158–1167.
- [14] E. Levy, et al., Mutation of the Alzheimer's disease amyloid gene in hereditary cerebral hemorrhage, Dutch type, *Science* 248 (4959) (1990) 1124–1126.
- [15] C. Van Broeckhoven, et al., Amyloid beta protein precursor gene and hereditary cerebral hemorrhage with amyloidosis (Dutch), *Science* 248 (4959) (1990) 1120–1122.
- [16] F. Prelli, et al., Expression of a normal and variant Alzheimer's beta-protein gene in amyloid of hereditary cerebral hemorrhage, Dutch type: DNA and protein diagnostic assays, *Biochem. Biophys. Res. Commun.* 170 (1) (1990) 301–307.
- [17] O. Bugiani, et al., Hereditary cerebral hemorrhage with amyloidosis associated with the E693K mutation of APP, *Arch. Neurol.* 67 (8) (2010) 987–995.
- [18] S.G. van Duinen, et al., Hereditary cerebral hemorrhage with amyloidosis in patients of Dutch origin is related to Alzheimer disease, *Proc. Natl. Acad. Sci. USA*, 84 (16) (1987) 5991–5994.
- [19] W. Luyendijk, et al., Hereditary cerebral haemorrhage caused by cortical amyloid angiopathy, *J. Neurol. Sci.* 85 (3) (1988) 267–280.
- [20] A.R. Wattendorff, et al., Hereditary cerebral haemorrhage with amyloidosis, Dutch type (HCHWA-D): clinicopathological studies, *J. Neurol. Neurosurg. Psychiatry* 58 (6) (1995) 699–705.
- [21] T.J. Grabowski, et al., Novel amyloid precursor protein mutation in an Iowa family with dementia and severe cerebral amyloid angiopathy, *Ann. Neurol.* 49 (6) (2001) 697–705.
- [22] Y. Shin, et al., Vascular changes in Iowa-type hereditary cerebral amyloid angiopathy, *Ann N Y Acad. Sci.* 977 (2002) 245–251.
- [23] Y. Tomidokoro, et al., Iowa variant of familial Alzheimer's disease: accumulation of posttranslationally modified AbetaD23N in parenchymal and cerebrovascular amyloid deposits, *Am. J. Pathol.* 176 (4) (2010) 1841–1854.
- [24] T. Mok, et al., Familial cerebral amyloid angiopathy due to the Iowa mutation in an Irish family, *Can. J. Neurol. Sci.* 41 (4) (2014) 512–517.
- [25] R. Nante, et al., Dementia in hereditary cerebral hemorrhage with amyloidosis-Dutch type is associated with cerebral amyloid angiopathy but is independent of plaques and neurofibrillary tangles, *Ann. Neurol.* 50 (6) (2001) 765–772.
- [26] J. Davis, et al., Early-onset and robust cerebral microvascular accumulation of amyloid beta-protein in transgenic mice expressing low levels of a vasculotropic Dutch/Iowa mutant form of amyloid beta-protein precursor, *J. Biol. Chem.* 279 (19) (2004) 20296–20306.

- [27] M.C. Herzog, et al., Abeta is targeted to the vasculature in a mouse model of hereditary cerebral hemorrhage with amyloidosis, *Nat. Neurosci.* 7 (9) (2004) 954–960.
- [28] B. Readhead, et al., Molecular systems evaluation of oligomeric APP(E693Q) and fibrillogenic APP(KM670/671NL)/PSEN1(Deltaexon9) mouse models identifies shared features with human Alzheimer's brain molecular pathology, *Mol. Psychiatry* 21 (8) (2016) 1153–1154.
- [29] J. Miao, et al., Cerebral microvascular amyloid beta protein deposition induces vascular degeneration and neuroinflammation in transgenic mice expressing human vasculotropic mutant amyloid beta precursor protein, *Am. J. Pathol.* 167 (2) (2005) 505–515.
- [30] J. Miao, et al., Reducing cerebral microvascular amyloid-beta protein deposition diminishes regional neuroinflammation in vasculotropic mutant amyloid precursor protein transgenic mice, *J. Neurosci.* 25 (27) (2005) 6271–6277.
- [31] F. Xu, et al., Early-onset subicular microvascular amyloid and neuroinflammation correlate with behavioral deficits in vasculotropic mutant amyloid beta-protein precursor transgenic mice, *Neuroscience* 146 (1) (2007) 98–107.
- [32] W. Xu, et al., Cerebral microvascular rather than parenchymal amyloid-beta protein pathology promotes early cognitive impairment in transgenic mice, *J. Alzheimers Dis.* 38 (3) (2014) 621–632.
- [33] J. Davis, et al., A Novel Transgenic Rat Model of Robust Cerebral Microvascular Amyloid with Prominent Vasculopathy, *Am. J. Pathol.* 188 (12) (2018) 2877–2889.
- [34] X. Zhu, et al., Robust neuroinflammation and perivascular pathology in rTg-DI rats, a novel model of microvascular cerebral amyloid angiopathy, *J. Neuroinflamm.* 17 (1) (2020) 78.
- [35] D.L. Popescu, W.E. Van Nostrand, J.K. Robinson, Longitudinal cognitive decline in a novel rodent model of cerebral amyloid angiopathy Type-1, *Int. J. Mol. Sci.* 21 (7) (2020).
- [36] H. Lee, et al., Diffuse white matter loss in a transgenic rat model of cerebral amyloid angiopathy, *J. Cereb. Blood Flow Metab.* (2020), p. 271678X20944226.
- [37] W.E. Van Nostrand, et al., Protease nexin-II, a potent antichymotrypsin, shows identity to amyloid beta-protein precursor, *Nature* 341 (6242) (1989) 546–549.
- [38] K. Johnson-Wood, et al., Amyloid precursor protein processing and A beta42 deposition in a transgenic mouse model of Alzheimer disease, *Proc. Natl. Acad. Sci. U.S.A.* 94 (4) (1997) 1550–1555.
- [39] R.B. DeMattos, et al., Clusterin promotes amyloid plaque formation and is critical for neurotoxicity in a mouse model of Alzheimer's disease, *Proc. Natl. Acad. Sci. USA* 99 (16) (2002) 10843–10848.
- [40] B.V. Zlokovic, et al., Differential expression of Na,K-ATPase alpha and beta subunit isoforms at the blood-brain barrier and the choroid plexus, *J. Biol. Chem.* 268 (11) (1993) 8019–8025.
- [41] R. Deane, et al., RAGE mediates amyloid-beta peptide transport across the blood-brain barrier and accumulation in brain, *Nat. Med.* 9 (7) (2003) 907–913.
- [42] G. Gomori, *Microtechnical demonstration of Iron: a criticism of its methods*, *Am. J. Pathol.* 12 (5) (1936), p. 655–664 1.
- [43] J. Rungby, et al., The von Kossa reaction for calcium deposits: silver lactate staining increases sensitivity and reduces background, *Histochem. J.* 25 (6) (1993) 446–451.
- [44] J.M. Long, et al., Stereological estimation of total microglia number in mouse hippocampus, *J. Neurosci. Methods* 84 (1–2) (1998) 101–108.
- [45] M. Mullan, et al., A pathogenic mutation for probable Alzheimer's disease in the APP gene at the N-terminus of beta-amyloid, *Nat. Genet.* 1 (5) (1992) 345–347.
- [46] J. Davis, W.E. Van Nostrand, Enhanced pathologic properties of Dutch-type mutant amyloid beta-protein, *Proc. Natl. Acad. Sci. USA* 93 (7) (1996) 2996–3000.
- [47] W.E. Van Nostrand, et al., Pathogenic effects of D23N Iowa mutant amyloid beta-protein, *J. Biol. Chem.* 276 (35) (2001) 32860–32866.
- [48] H.V. Vinters, et al., Secondary microvascular degeneration in amyloid angiopathy of patients with hereditary cerebral hemorrhage with amyloidosis, Dutch type (HCHWA-D), *Acta Neuropathol.* 95 (3) (1998) 235–244.
- [49] F. Sellal, et al., *APP mutations in cerebral amyloid angiopathy with or without cortical calcifications: report of three families and a literature review*, *J. Alzheimers Dis.* 56 (1) (2017) 37–46.
- [50] L. Grand Moursel, et al., Osteopontin and phospho-SMAD2/3 are associated with calcification of vessels in D-CAA, an hereditary cerebral amyloid angiopathy, *Brain Pathol.* 29 (6) (2019) 793–802.
- [51] M.F. Lanfranco, et al., Expression and secretion of apoE isoforms in astrocytes and microglia during inflammation, *Glia* 69 (6) (2021) 1478–1493.
- [52] Y. Yamazaki, et al., Apolipoprotein E and Alzheimer disease: pathobiology and targeting strategies, *Nat. Rev. Neurol.* 15 (9) (2019) 501–518.
- [53] K. Rannikmae, et al., APOE associations with severe CAA-associated vasculopathic changes: collaborative meta-analysis, *J. Neurol. Neurosurg. Psychiatry* 85 (3) (2014) 300–305.
- [54] K. Garai, et al., The binding of apolipoprotein E to oligomers and fibrils of amyloid-beta alters the kinetics of amyloid aggregation, *Biochemistry* 53 (40) (2014) 6323–6331.
- [55] T. Islam, et al., Apolipoprotein E impairs amyloid-beta fibril elongation and maturation, *FEBS J.* 287 (6) (2020) 1208–1219.
- [56] F. Xu, et al., Human apolipoprotein E redistributes fibrillar amyloid deposition in Tg-SwDI mice, *J. Neurosci.* 28 (20) (2008) 5312–5320.
- [57] M.P. Burns, et al., Co-localization of cholesterol, apolipoprotein E and fibrillar Abeta in amyloid plaques, *Brain Res. Mol. Brain Res.* 110 (1) (2003) 119–125.
- [58] F. Liao, et al., Murine versus human apolipoprotein E4: differential facilitation of and co-localization in cerebral amyloid angiopathy and amyloid plaques in APP transgenic mouse models, *Acta Neuropathol. Commun.* 3 (2015) 70.
- [59] K. Hsiao, et al., Correlative memory deficits, Abeta elevation, and amyloid plaques in transgenic mice, *Science* 274 (5284) (1996) 99–102.
- [60] C. Sturchler-Pierrat, et al., Two amyloid precursor protein transgenic mouse models with Alzheimer disease-like pathology, *Proc. Natl. Acad. Sci. USA* 94 (24) (1997) 13287–13292.
- [61] M.E. Calhoun, et al., Neuronal overexpression of mutant amyloid precursor protein results in prominent deposition of cerebrovascular amyloid, *Proc. Natl. Acad. Sci. USA* 96 (24) (1999) 14088–14093.
- [62] R. Deane, et al., LRP/amyloid beta-peptide interaction mediates differential brain efflux of Abeta isoforms, *Neuron* 43 (3) (2004) 333–344.
- [63] R.O. Weller, et al., Perivascular drainage of amyloid-beta peptides from the brain and its failure in cerebral amyloid angiopathy and Alzheimer's disease, *Brain Pathol.* 18 (2) (2008) 253–266.
- [64] E.N. Bakker, et al., *Lymphatic clearance of the brain: perivascular, paravascular and significance for neurodegenerative diseases*, *Cell. Mol. Neurobiol.* 36 (2) (2016) 181–194.
- [65] J.L. Jankowsky, H. Zheng, Practical considerations for choosing a mouse model of Alzheimer's disease, *Mol. Neurodegener.* 12 (1) (2017) 89.
- [66] Z.S.Y. Lok, A.N. Lyle, Osteopontin in vascular disease, *Arterioscler. Thromb. Vasc. Biol.* 39 (4) (2019) 613–622.
- [67] F. Kahles, H.M. Findeisen, D. Brummer, *Osteopontin: a novel regulator at the cross roads of inflammation, obesity and diabetes*, *Mol. Metab.* 3 (4) (2014) 384–393.